Astron. Astrophys. 278, 328–339 (1993)

ASTRONOMY AND ASTROPHYSICS

Iterative image reconstruction from the bispectrum*

K.-H. Hofmann and G. Weigelt

Max-Planck-Institut für Radioastronomie, Auf dem Hügel 69, D-53121-Bonn, Germany

Received March 26, accepted May 29, 1993

Abstract. We present iterative least-squares methods for reconstructing diffraction-limited images from the object bispectrum obtained by speckle masking (bispectral analysis) and from other Fourier data. The theory and first astronomical speckle masking applications are described. An approximation of the least-squares integral is derived which makes it possible to calculate easily
thousands of iterations with images of 512x512 pixels. Various extensions of the basic method to the simultaneous treatment of many object pixels are dicussed. Finally, applications of modified versions of the method to the Knox-Thompson method, shearing interferometry, deconvolution of aberrated images, optical long-baseline interferometry, radio interferometry (especially, mm- and submm-interferometry) and other methods are discussed.

Key words: image processing – interferometry – observational methods

1. Introduction

The atmosphere of the earth restricts the resolution of conventional astronomical photography to $\sim 0\farcs5$ to $1''$. Much higher resolution can be obtained by various speckle methods, which yield diffraction-limited resolution, for example, $\sim 0\farcs03$ for a 3.6-m telescope and $\lambda = 500$nm. A long list of references for speckle methods is given in the review articles by Dainty (1984), Roddier (1981), and Weigelt (1991). Speckle masking (Weigelt 1977; Weigelt & Wirnitzer 1983; Lohmann et al. 1983; Hofmann & Weigelt 1986a), is a speckle method based on triple correlation or bispectrum processing. It can reconstruct both the modulus and the phase of the object Fourier transform from a sequence of speckle interferograms. Therefore, true diffraction-limited images of general astronomical objects can be obtained. Speckle masking can also be applied to optical long-baseline interferometers since it can measure all closure phases, even in the multi-speckle case (if telescope diameter $\gg$ Fried parameter r_0). In speckle masking first the ensemble average bispectrum of all speckle interferograms is calculated. After compensation of photon bias terms (Wirnitzer 1985; Pehlemann et al. 1992) or photon-counting hole terms (Hofmann 1990, 1992), and after the compensation of the speckle masking transfer function the object bispectrum

$$O^{(3)}(u,v) = O(u)\,O(v)\,O(-u-v) \tag{1}$$

is obtained up to the cut-off frequency of the telescope. $O(u)$ denotes the diffraction-limited Fourier transform of the object $o(x)$. The variable x is a *2-dimensional* coordinate vector in object space, u and v are *2-dimensional* coordinate vectors in Fourier space. From the *4-dimensional* object bispectrum $O^{(3)}(u,v)$ a diffraction-limited image of the object $o(x)$ can be reconstructed. In the conventional recursive image reconstruction method, the Fourier phase of the object is extracted in a recursive way from its bispectrum phases.

In this paper, we discuss an iterative least-squares algorithm for reconstructing a diffraction-limited image of the object from the speckle masking bispectrum. The algorithm, called building block method (Hofmann & Weigelt 1990a, 1990b, 1992; Morita 1991), is an extension of the gridfit method (Pauliny-Toth et al. 1976) used in radio interferometry. Morita (1991) has performed an experiment with mm-data, in which the combination of speckle masking and the building block method yielded better reconstructions than hybrid mapping or self-calibration. The building block method avoids complicated bispectrum phase integration (as in the recursive method) since it searches directly for that positive diffraction-limited image of the object which has the best agreement with the bispectrum measured. The image of iteration step $k+1$ is produced by adding a single $(k+1)$th diffraction-limited point-spread function (psf) to the image of iteration step k. The psf is added at such a position that the distance (difference) between the bispectrum of the new image and the measured bispectrum is as small as possible. Other least-squares algorithms for image reconstruction from the bispectrum were proposed by Lannes (1988, 1990), Meng et al. (1990), Marron et al. (1990), Cornwell (1987), Gorham et al. (1989), Haniff (1990), and Takajo & Takahashi (1991). In Sect. 2 we describe the theory of the building block method.

Send offprint requests to: K.-H. Hofmann

* Based on observations at the European Southern Observatory, La Silla, Chile.

In Sect. 3 we discuss the application of the method to different high-resolution imaging methods. In Sect. 4 we describe modifications of the method. Finally, in Sect. 5 we describe applications to computer-simulated and real astronomical speckle interferograms. The experiments suggest that in some cases the building block method yields better reconstructions than the recursive method, especially in the case of optical long-baseline interferometers (Reinheimer et al. 1992, 1993).

2. Theory of the iterative building block method

In incoherent imaging, any object intensity distribution $o_k(x)$ can be described by a sum of many identical and positive point-spread functions (psfs) $t(x)$:

$$o_k(x) = \sum_{m=1}^{k} t(x - x_m), \tag{2}$$

where x_m denotes the position of the m-th psf and k is the total number of psfs ($x_n = x_m$ may be possible for $n \neq m$). We can say that the image $o_k(x)$ is built up by many identical building blocks $t(x)$. A complicated object requires many building blocks. In the building block method the high-resolution image of the object is built up sequentially, iteration step by iteration step, by many building blocks $t(x)$.

The goal of the proposed algorithm is the derivation of $o(x)$ from the object bispectrum $O^{(3)}(u, v)$ measured by speckle masking. The proposed image reconstruction algorithm searches for the positive diffraction-limited image of the object whose bispectrum has the best agreement with the bispectrum measured. The image of the first iteration step consists of one building block $t(x)$ located at any arbitrary position, for example at the centre of the image field. The position of the first building block may be chosen arbitrarily since the bispectrum contains no information about the position of the object (shift-invariance of the bispectrum). The image $o_{k+1}(x)$ of iteration step $k + 1$ is produced by adding one building block $t(x)$ at position $x = x'$ to image $o_k(x)$ of iteration step k, i.e.

$$o_{k+1}(x; x') := o_k(x) + t(x - x'). \tag{3}$$

The position x' of the $(k + 1)$th building block is chosen such that the distance (difference) $d_{k+1}(x')$ between the measured bispectrum $O^{(3)}(u, v)$ and the bispectrum $O^{(3)}_{k+1}(u, v; x')$ of the image $o_{k+1}(x; x')$ is as small as possible. The distance $d_{k+1}(x')$ is defined as

$$d_{k+1}(x') := \int | O^{(3)}_{k+1}(u, v; x') - O^{(3)}(u, v) |^2 \, \mathrm{d}u \, \mathrm{d}v, \tag{4}$$

with $O^{(3)}_{k+1}(0, 0; x') = O^{(3)}(0, 0) = 1$. The image with the smallest distance value has the best agreement with the measured data $O^{(3)}(u, v)$. If the absolute minimum of the distance function $d_{k+1}(x')$ lies at position $x' = x'_{\min}$, the image of the best agreement with $O^{(3)}(u, v)$ is $o_{k+1}(x; x' = x'_{\min}) =: o_{k+1}(x)$.

Because the amount of noise is different in different parts of the bispectrum measured, a weight function $w(u, v)$ should be used in the above distance and Eq. (4) can be replaced by

$$d_{k+1}(x') = \int | w(u, v) \, [O^{(3)}_{k+1}(u, v; x') - O^{(3)}(u, v)] \, |^2 \, \mathrm{d}u \, \mathrm{d}v. \tag{5}$$

A successfull realization of such a weight function is a Wiener type weight filter (Pratt 1978). In this case the weight function applied to the bispectrum difference $O^{(3)}_{k+1}(u, v) - O^{(3)}(u, v)$ can be described by

$$w(u, v) = \frac{|O^{(3)}_{k+1}(u, v) - O^{(3)}(u, v)|^2}{|O^{(3)}_{k+1}(u, v) - O^{(3)}(u, v)|^2 + var\{O^{(3)}(u, v)\}}. \tag{6}$$

$var\{O^{(3)}(u, v)\}$ denotes the variance of the noisy bispectrum $O^{(3)}(u, v)$

For increasing the speed of the calculation of the distance function $d_{k+1}(x')$, an approximated expression of $d_{k+1}(x')$ is used. This approximation is based on the fact that changes introduced by the addition of a further building block are very small when $o_k(x)$ already consists of a large number k of building blocks. The approximated expression of the distance function is derived in Appendix A. The approximation of the distance function $d_{k+1}(x')$ has the form

$$\begin{aligned} d_{k+1}(x') \approx\ & d_k \\ & + 6/k \int |w(u, v)|^2 \, [O^{(3)}_k(-u, -v) - O^{(3)}(-u, -v)] \\ & \times O_k(u) \, O_k(v) \\ & \times \exp\{2\pi i (u + v) \cdot x'\} \, \mathrm{d}u \, \mathrm{d}v \,, \end{aligned} \tag{7}$$

with $i = \sqrt{-1}$. $O_k(u)$ denotes the normalized ($O_k(0) = 1$) Fourier transform of the image $o_k(x)$ calculated at iteration step k, $O^{(3)}_k(u, v)$ is the bispectrum of $o_k(x)$, and d_k denotes the distance between the measured bispectrum $O^{(3)}(u, v)$ and the bispectrum $O^{(3)}_k(u, v)$ of $o_k(x)$. The iteration step $k+1$ described above can be summarized as follows:

1. Calculation of the distance function $d_{k+1}(x')$ using the approximation given in Eq. (7).
2. Determination of the position $x'_{\min}$ of the absolute minimum of the distance function.
3. Generation of the new $(k+1)$th image $o_{k+1}(x)$ by adding one building block $t(x)$ at the position $x'_{\min}$ to the previous image $o_k(x)$ (all building blocks used in the described algorithm have the same intensity; modified methods are described in Sect. 4).

Many iteration steps (~ 100 to 10^4) are required for the reconstruction of a high-resolution image of the object. The number of required iterations depends on the complexity of the object. In Appendix B is shown that the method converges to the correct image of the object.

3. Application of the building block method to various imaging methods

In this section we discuss applications of the building block method to various high-resolution imaging methods. We briefly

discuss the application of the method to speckle interferometry (Labeyrie 1970), the Knox-Thompson method (Knox & Thompson 1974), imaging shearing interferometry (Hofmann & Weigelt 1986b; Roddier & Roddier 1986; Ribak 1987), optical long-baseline interferometry (Reinheimer et al. 1992, 1993), non-redundant masking (Baldwin et al. 1986; Readhead et al. 1988; Nakajima et al. 1989), radio interferometric imaging, the deconvolution of HST images and other aberrated images, and to tomographic image reconstruction techniques.

3.1. Application to speckle interferometry

In speckle interferometry the required distance function can be described by

$$d_{k+1}(x') = \int \left| |O(u)|^2 - |O_{k+1}(u;x')|^2 \right|^2 \mathrm{d}u, \qquad (8)$$

where $|O(u)|^2$ denotes the measured object power spectrum and $|O_{k+1}(u;x')|^2$ is the power spectrum of the model object $o_{k+1}(x;x') = o_k(x) + t(x - x')$. Because of the missing phase information the building block method yields the power spectrum or autocorrelation function of the object.

3.2. Application to the Knox-Thompson method

In the Knox-Thompson method the following distance function has to be minimized:

$$d_{k+1}(x') = \int \left| O(u)O^*(u+\Delta u) - O_{k+1}(u;x')O^*_{k+1}(u+\Delta u;x') \right|^2 \mathrm{d}u\,\mathrm{d}\Delta u. \qquad (9)$$

$O(u)O^*(u+\Delta u)$ denotes the Knox-Thompson spectrum which can be calculated with different shift vectors Δu up to $|\Delta u| \lesssim r_0/\lambda$ (r_0=Fried parameter). $O_{k+1}(u;x')$ is the Fourier transform of the model object $o_{k+1}(x;x') = o_k(x) + t(x - x')$.

3.3. Application to imaging shearing interferometry

In imaging shearing interferometry a subset of the total bispectrum of the object is obtained. The distance function has the same form as described in Eqs. (5) and (7).

3.4. Application to optical long-baseline interferometry (single and multi-speckle case)

In this case (see Reinheimer et al. 1992, 1993) the distance function is given by

$$d_{k+1}(x') = \int \left| \hat{O}^{(3)}(u,v) - \hat{O}^{(3)}_{k+1}(u,v;x') \right|^2 \mathrm{d}u\,\mathrm{d}v, \qquad (10)$$

where $\hat{O}^{(3)}(u,v)$ describes the subset of all bispectrum elements for coordinates (u,v) where $< \hat{P}^{(3)}(u,v) >$ has values greater than zero ($< \hat{P}^{(3)}(u,v) >$ is the diluted bispectrum or speckle masking transfer function) and $\hat{O}^{(3)}_{k+1}(u,v;x')$ is the bispectrum of the model object $o_{k+1}(x;x') = o_k(x) + t(x - x')$. The large gaps in the Fourier data of optical long-baseline interferometers cause large gaps in $< \hat{P}^{(3)}(u,v) >$. Speckle masking and the building block method can be applied in both cases, the single-speckle case (r_0-apertures; r_0=Fried parameter) and in the multi-speckle case (telescope diameters $\gg r_0$). In the multi-speckle case the interferograms consist of many speckles with crossed fringes in each speckle. Successful applications of the building block method to simulated long-baseline interferograms (multi-speckle case) were described by Reinheimer et al. (1992, 1993).

3.5. Application to the non-redundant mask method (single-speckle case)

In the non-redundant mask method (Baldwin et al. 1986; Readhead et al. 1988; Nakajima et al. 1989), the distance function is the same as in Sect. 3.4.

3.6. Application to radio interferometry

In radio interferometry an image of the object is usually derived from the complex visibilities of many antenna pairs by self-calibration imaging methods (Readhead & Wilkinson 1978; Cornwell & Wilkinson 1981; Schwab 1980; Cornwell 1989 and references therein). In these methods the closure phases are not determined explicitly but the phase closure information is used implicitly in the iterative image reconstruction methods (see discussion in Cornwell 1989).

An alternative to the self-calibration method consists of the following three steps:
(1) First the ensemble average bispectrum of the visibilities recorded in many short coherence times at the same uv-points is calculated (the phases of the bispectrum are the closure phases). This technique is advantageous for very faint objects since bispectra can be averaged until good SNR is achieved (Lohmann et al. 1983; Cornwell 1987, 1989). It is a limitation of self-calibration that the measurements of the coherence phase must have a SNR >1 in the atmospheric coherence time (see Cornwell 1989).
(2) In the average bispectrum it is possible to compensate noise bias terms to obtain the compensated object bispectrum (Wirnitzer 1985; Pehlemann et al. 1992).
(3) From the compensated object bispectrum a diffraction-limited image can be reconstructed by the building block method.
Morita (1991) has performed an experiment with mm-data, in which the combination of speckle masking and the building block method yielded better reconstructions than hybrid mapping or self-calibration.

3.7. Application to the deconvolution of HST images and other aberrated images

In this case the distance function can be described by

$$d_{k+1}(x') = \int |\, I(u) - O_{k+1}(u; x')\, P(u) \,|^2 \, \mathrm{d}u. \qquad (11)$$

$I(u)$ is the Fourier transform of the HST image degraded by spherical aberration and by photon noise, and $O_{k+1}(u; x')$ denotes the Fourier transform of the model object $o_{k+1}(x; x') = o_k(x) + t(x - x')$ obtained after iteration step $k + 1$. $P(u)$ is the Fourier transform of the aberrated psf. $P(u)$ is derived from measurements of an unresolved star.

3.8. Application to tomography

The building block method can be applied to tomographic image reconstruction techniques as used, for example, in medical imaging and in some astronomical techniques. In this case the projections of the object recorded under many different orientation angles are compared with the same projections of the model object $o_k(x)$. A first application of this method to speckle masking was described by Hofmann & Weigelt (1990a, 1990b).

4. Modifications of the building block method

In this section we discuss various modifications of the basic method described in Sect. 2.

4.1. Two or more building blocks simultaneously

In this technique a new model object o_{k+1} is produced by simultaneously adding two or more building blocks to the image of the previous iteration step, i.e. $o_{k+1}(x; x'_1, x'_2, ...) = o_k(x) + t(x - x'_1) + t(x - x'_2) + ...$ The distance is here a function of two or more variables $x'_1, x'_2, ...$, which are the position vectors of the new building blocks (i.e. $d_{k+1}(x'_1, x'_2, ...)$).

4.2. Building blocks with varying intensities

In this case the position x' **and** the intensity α of the new building block has to be determined simultaneously. The new model object is $o_{k+1}(x; x', \alpha) = o_k(x) + \alpha\, t(x - x')$. The distance is here a function of both, the position x' and the intensity α of the new building block (i.e. $d_{k+1}(x', \alpha)$).

4.3. Testing all possible images

The most attractive image reconstruction procedure would be to test all possible images. However testing of all possible images is not feasible for most objects because of too long computing times (with the exception of very compact objects). If the object consists, for example, of 6 pixels and if we work with 10 different intensity quantisation levels, then there exist already 10^6 different images. If testing of one image requires 0.1 sec computing time, testing of 10^6 images require ~ 28 hours computing time. In the case of 8 pixels the computing time is already 116 days. Testing of one image means to compare the bispectrum of the model object with the measured bispectrum (by calculating the least-squares difference). On the other hand testing all possible intensity *correction functions* is feasible. As an example, consider a star cluster of 20 stars (or another image consisting of 20 pixels). Small intensity corrections, for example, mean: the intensites of all stars can be changed simultaneously by adding or subtracting one small intensity building block to each star. In this case $2^{20} \sim 10^6$ possible correction functions have to be tested. Repeating this procedure (1 cycle) several times with smaller and smaller building blocks is useful. The whole process can be done by fast computers (~ 3 days for 3 cycles and ~ 0.1 sec per correction function).

4.4. Using a robust estimator instead of a least-squares estimator

Many methods proposed for reconstructing high-resolution images of the object are based on the least-squares technique. A reconstruction procedure based on robust regression techniques was proposed by Freeman et al. (1992). Robust regression was applied to the estimation of binary star parameters from the Fourier spectrum measured by the Knox-Thompson method. The results suggest that the robust regression solution is superior to the least-squares solution. We propose the application of a robust regression algorithm to the determination of object parameters or to the calculation of the object directly from the bispectrum measured. If the observed object is, for example, a binary star, the object parameters (i.e. the intensities and positions of the two stars; see also Glindemann et al. 1992) can be derived from the bispectrum measured and the binary star model bispectrum by a robust regression algorithm similar to that used by Freeman et al. (1992). Robust regression may also be implemented to the building block method. To this end the least-squares estimator of the building block method (see Eq. (4)) has to be replaced by a robust estimator, for example, the median. The discrete description of the distance function with the conventional least-squares estimator in the building block method is given by

$$d^{\mathrm{LS}}_{k+1}(x') = \sum_{u,v} |O^{(3)}_{k+1}(u, v; x') - O^{(3)}(u, v)|^2, \qquad (12)$$

where u and v denote discrete Fourier space coordinates describing the set of all measured bispectrum elements. The distance function described with the median, one robust estimator, has the form

$$d^{\mathrm{med}}_{k+1}(x') = \mathrm{med}_{u,v}\{|O^{(3)}_{k+1}(u, v; x') - O^{(3)}(u, v)|\}, \qquad (13)$$

where $\mathrm{med}_{u,v}\{|...|\}$ denotes the median over all square root differences $|O^{(3)}_{k+1}(u, v; x') - O^{(3)}(u, v)|$. This estimator is robust since it does not take into account outliers of the noisy bispectrum difference. The least-squares estimator does not reject such outliers.

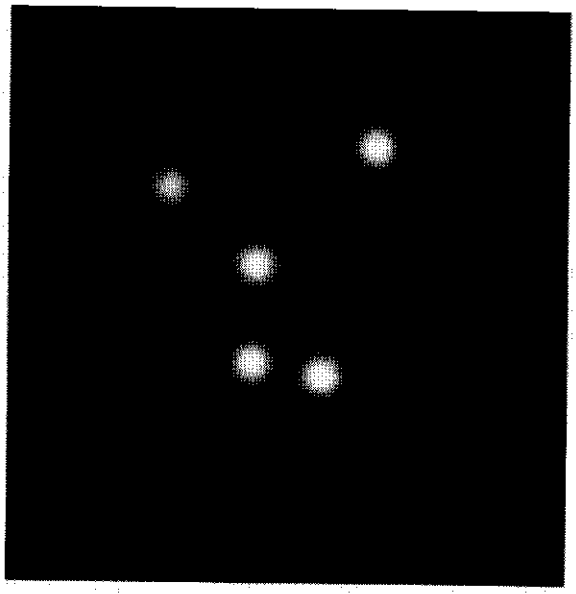

Fig. 1. Object of the computer experiment

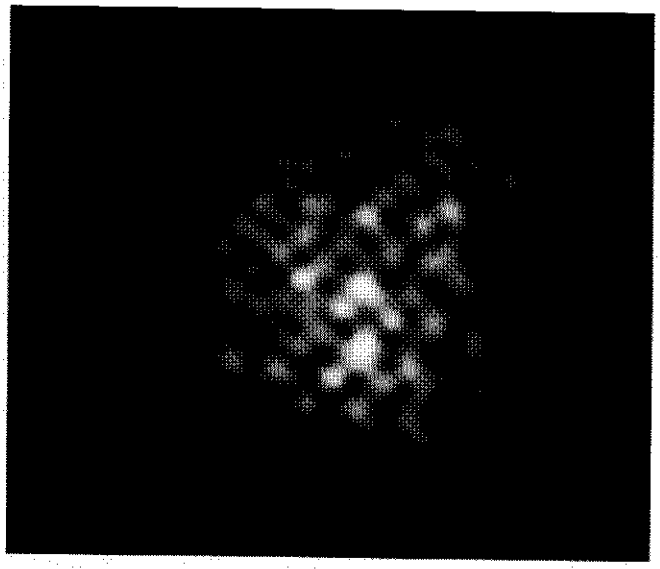

Fig. 2. One of the 30 000 object speckle interferograms without photon noise

4.5. Using other elementary functions instead of psfs

In the basic building block method the image is built up by many identical psfs. In the case of extended objects other sets of elementary functions, as for example spherical harmonics or cosine functions (Fourier synthesis), may be more appropriate.

5. Experimental results

Figures 1 to 11 illustrate the feasibility of the building block method. We have performed three different image reconstruction experiments. The first experiment was performed with computer generated speckle interferograms (Sect. 5.1), the second one with speckle interferograms of the double star ω Leonis (Sect. 5.2), and the third one with speckle interferograms of

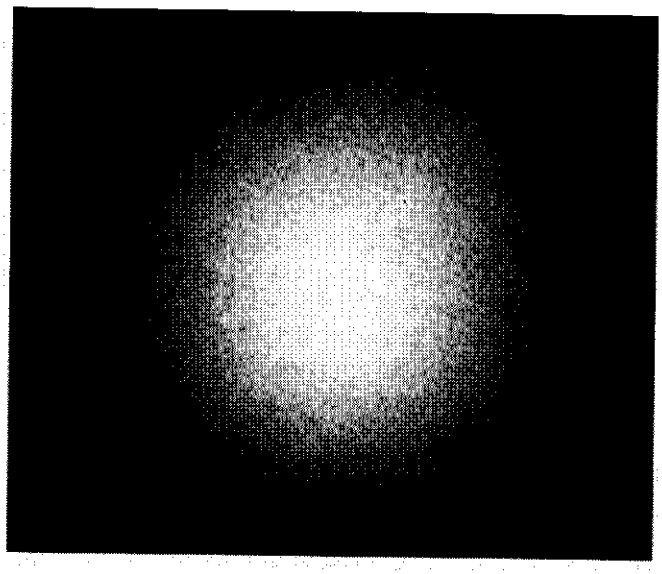

Fig. 3. Long-exposure image reconstructed from 10 000 simulated object speckle interferograms with photon noise corresponding to 50 photoevents/frame

η Carinae (Sect. 5.3). The speckle data for the last two experiments were taken with the 2.2-m ESO/MPG telescope at La Silla, Chile.

5.1. Experiments with computer-generated speckle interferograms

30 000 point source speckle interferograms were generated as follows. First a random wavefront was produced to simulate the atmosphere of the earth. Random gaussian distributed numbers were calculated and the convolution with the covariance function of the optical path fluctuations as described by Roddier (1981) was applied to obtain a random wavefront. Then the random wavefront was multiplied with the simulated telescope pupil function. After a subsequent Fourier transform and modulus square operation the intensity distribution of the point source speckle interferogram was obtained. A 2.2-m telescope at λ=500nm (diffraction-limited resolution of $\sim 0\farcs05$) and a seeing of $\sim$ 0.5″was simulated. Speckle interferograms of an object were produced by convolving the point source speckle interferograms with the computer object, a cluster of five unresolved stars. Finally, the object speckle interferograms were degraded by photon noise (25, 50 and 100 photoevents per object speckle interferogram). For each photon noise level three independent data sets of 10 000 object speckle interferograms were produced. The generated speckle data sets were processed as follows.

Each data set was processed to obtain the average bispectrum and the average power spectrum. The photon bias terms in the average bispectrum and power spectrum were removed. After compensation of the speckle interferometry transfer function the object power spectrum was obtained. The compensation was performed with the average power spectrum of sin-

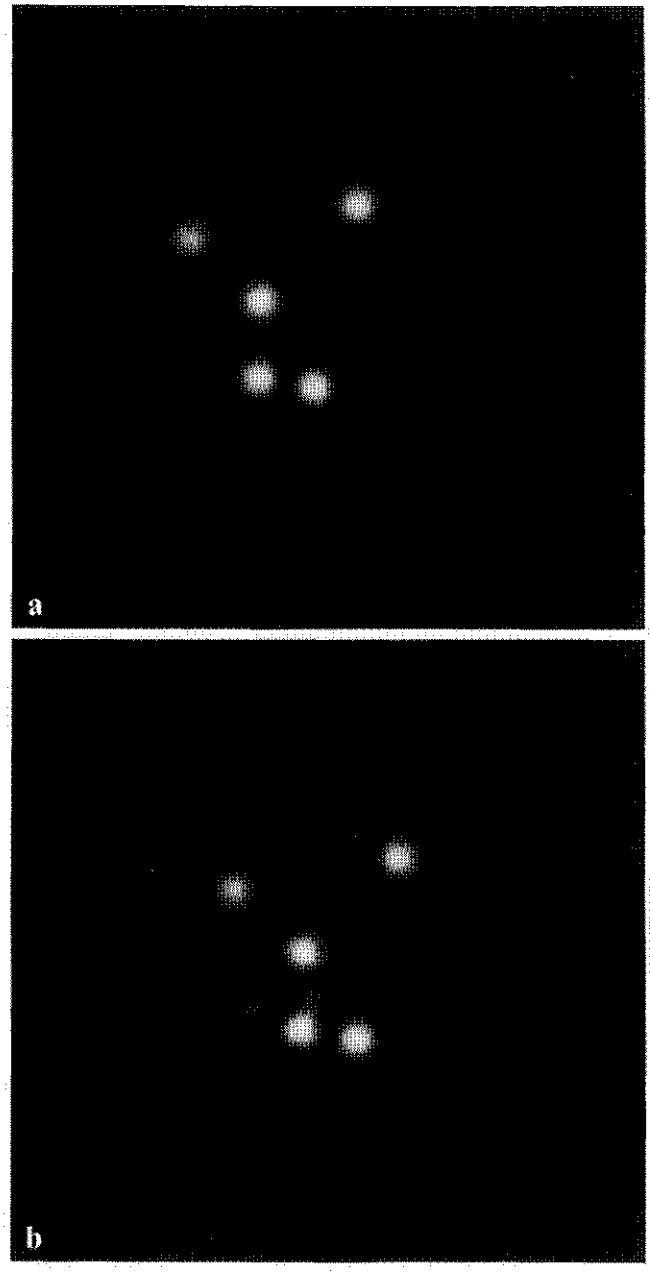

Fig. 4. a and b. Two typical images reconstructed from the average bispectrum obtained from 10 000 speckle interferograms with photon noise corresponding to ~100 photoevents/frame. **a** (top) is the diffraction-limited image reconstructed by the iterative building block method and 400 iteration steps (mean photometric error (average over all 5 stars): 4.0%). **b** (bottom) is the image obtained from the same bispectrum, but using the conventional recursive reconstruction method (mean photometric error: 6.8%)

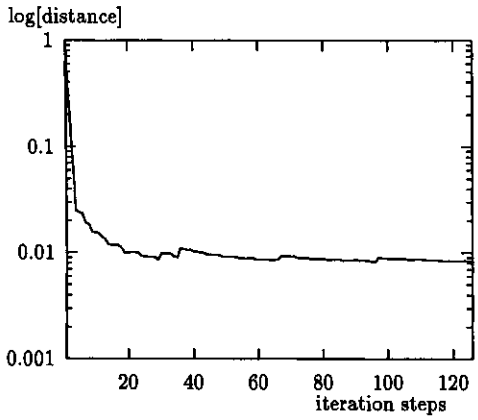

Fig. 5. Convergence curve of the building block reconstruction shown in Fig. 4a. The distance between the measured bispectrum and the bispectrum of the iterated image during the reconstruction process decreases with the number of iteration steps. The measured distance is displayed with a logarithmic scale (arbitrary scaling factor) as a function of the iteration steps

gle star speckle interferograms recorded under the same seeing conditions. From the object power spectrum $|O(u)|^2$ and the photon bias-compensated average bispectrum $< I^{(3)}(u,v) >$, the object bispectrum $O^{(3)}(u,v)$ was obtained in the following way: (1) from the object power spectrum $|O(u)|^2$ the modulus $|O^{(3)}(u,v)| = |O(u)|\,|O(v)|\,|O(-u-v)|$ of the object bispectrum was derived; (2) the object bispectrum $O^{(3)}(u,v)$ was obtained by combining $|O^{(3)}(u,v)|$ from step (1) with the phase of the average bispectrum $< I^{(3)}(u,v) >$. Object bispectrum and average bispectrum have the same phase since the average speckle masking transfer function does not affect the bispectrum phase (Lohmann et al. 1983). From the object bispectrum a diffraction-limited image of the object was reconstructed with the iterative image reconstruction algorithm presented in Sect. 2. The noise in the distance function $d_{k+1}(x')$ of the building block method was suppressed by the Wiener filtering procedure described in Sect. 2.

From the same object bispectrum a second diffraction-limited image was derived with the recursive method (Lohmann et al. 1983). For the recursive reconstruction of the object Fourier phase the bispectrum phases were weighted according to their quality (the signal-to-noise ratio of the phase of the average bispectrum was used as the weight function).

Figures 1 to 7 show the results of the computer experiment. Figure 1 is the computer object. Figure 2 shows one of the 30 000 generated speckle interferograms (three sets of 10 000 interferograms) of the object (without photon noise). Figure 3 is the long-exposure image derived from 10 000 simulated ob-

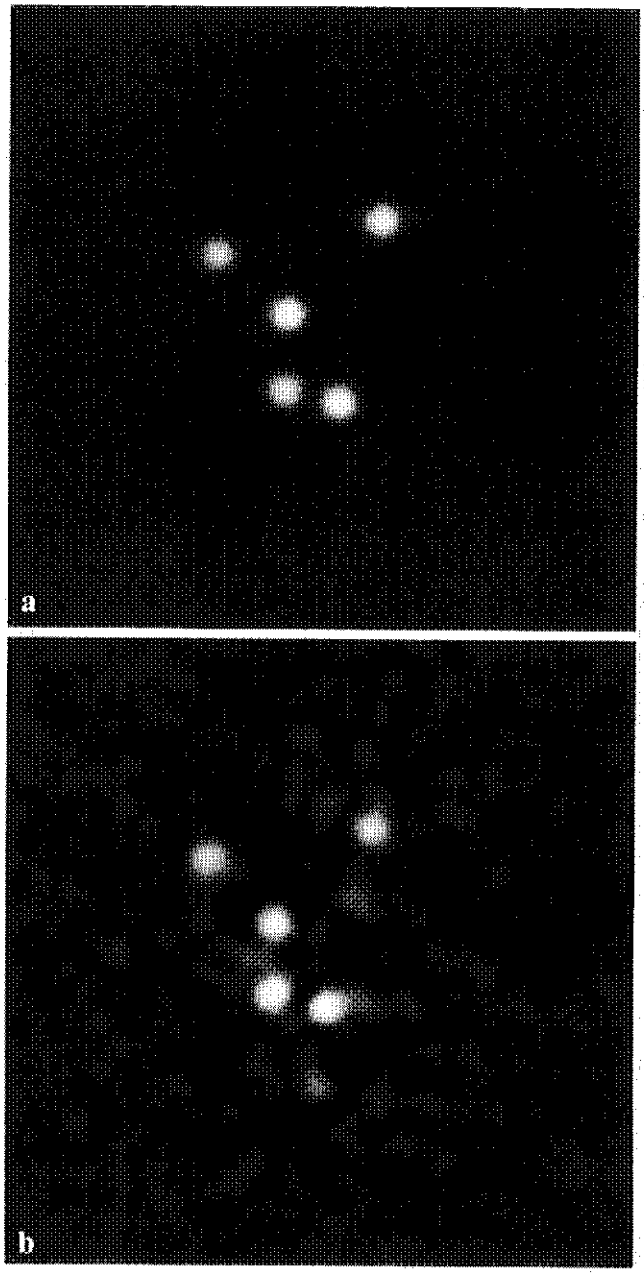

Fig. 6. a and b. Two typical images reconstructed from the average bispectrum obtained from 10000 speckle interferograms with photon noise corresponding to ~50 photoevents/frame. **a** (top) is the diffraction-limited image reconstructed by the iterative building block method and 400 iteration steps (mean photometric error: 6.1%). **b** (bottom) is the image obtained from the same bispectrum, but using the conventional recursive reconstruction method (mean photometric error: 12.1%)

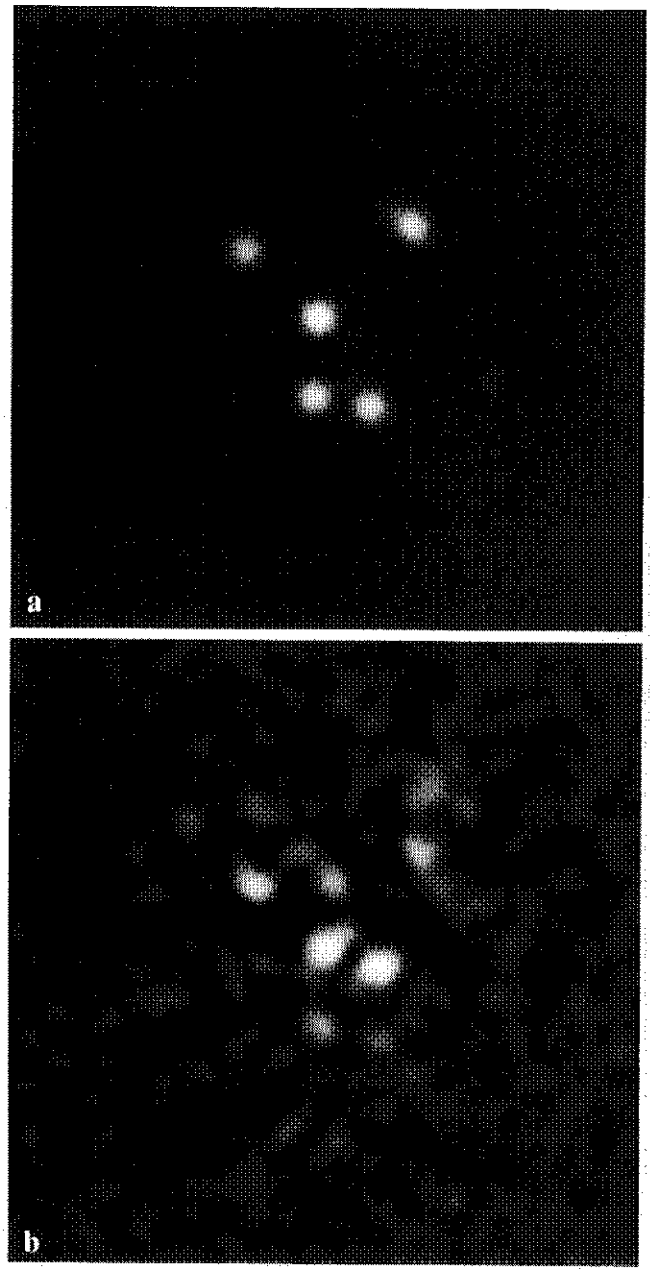

Fig. 7. a and b. Two typical images reconstructed from the average bispectrum obtained from 10000 speckle interferograms with photon noise corresponding to ~25 photoevents/frame. **a** (top) is the diffraction-limited image reconstructed by the iterative building block method and 400 iteration steps (mean photometric error: 13.3%). **b** (bottom) is the image obtained from the same bispectrum, but using the conventional recursive reconstruction method (because of too high noise level the mean photometric error could not be measured)

ject speckle interferograms with photon noise corresponding to 50 photoevents per interferogram. Figure 4 shows typical images reconstructed from the average bispectrum obtained from 10 000 speckle interferograms with photon noise corresponding to ~100 photoevents/frame. Figure 4a is the diffraction-limited reconstruction obtained with the iterative building block method and 400 iteration steps. Figure 4b shows the image reconstructed from the same average bispectrum by using the recursive reconstruction method. The plot in Fig. 5 illustrates the decreasing distance between the measured bispectrum and the bispectrum of the iterated image during the reconstruction of the image shown in Fig. 4a. The distance is displayed with a logarithmic scale as a function of the number of iteration steps. Figure 6 shows typical reconstructions obtained from 10 000 speckle interferograms with photon noise of ~50 photoevents/frame. Figure 6a is the diffraction-limited building block reconstruction with 400 iteration steps and Fig. 6b is the reconstruction obtained from the same average bispectrum by using the recursive method. Figures 7a and 7b show the building block reconstruction and the recursive reconstruction, respectively, obtained for 10 000 interferograms and 25 photoevents per frame. In this case the recursive reconstruction failed. Because the computer object is known (Fig. 1) the photometric accuracy of the reconstructed images can be determined. We have measured the relative photometric error of each of the five stars. The relative photometric error is the intensity error of each star divided by its true intensity. Averaging over all five stars yields the mean photometric error of the reconstructed image. Table 1 lists the mean photometric errors of the reconstructions. For each photon noise level (100, 50 and 25 photoevents/interferogram) three independent data sets (10 000 speckle interferograms per set) were produced. From each of the 9 data sets one image was reconstructed with the building block method and one with the recursive method. In Table 1 the mean photometric errors of all 18 reconstructions obtained at the photon noise levels 100, 50 and 25 photoevents per frame are listed. From all 3 data sets with photon noise corresponding to ~25 photoevents per frame the reconstruction of diffraction-limited images by the recursive method failed, but the building block method still worked. The mean photometric error of the building block reconstructions shown in Fig. 4a (100 photoevents/frame), Fig. 6a (50 photoevents/frame), and Fig. 7a (25 photoevents/frame) are 4.0%, 6.1% and 13.3%, respectively. The mean photometric error of the recursive reconstructions shown in Fig. 4b (100 photoevents/frame), and Fig. 6b (50 photoevents/frame) are 6.8% and 12.1%, respectively. The mean photometric error of Fig. 7b (25 photoevents/frame) could not be determined.

5.2. *Experiment with speckle data of ω Leonis*

Figures 8 to 10 show an application of the building block method to 100 speckle interferograms of the double star ω Leonis taken with the 2.2-m ESO/MPG telescope at $\lambda \sim 630$nm (bandwidth ~ 20nm). The data were recorded with the speckle camera described by Baier & Weigelt (1983). From the average bispectrum of 100 speckle interferograms the object bispectrum was derived as described in Sect. 5.1. Diffraction-limited images of ω Leonis were reconstructed from the object bispectrum by (a) the building block method and (b) the recursive method.

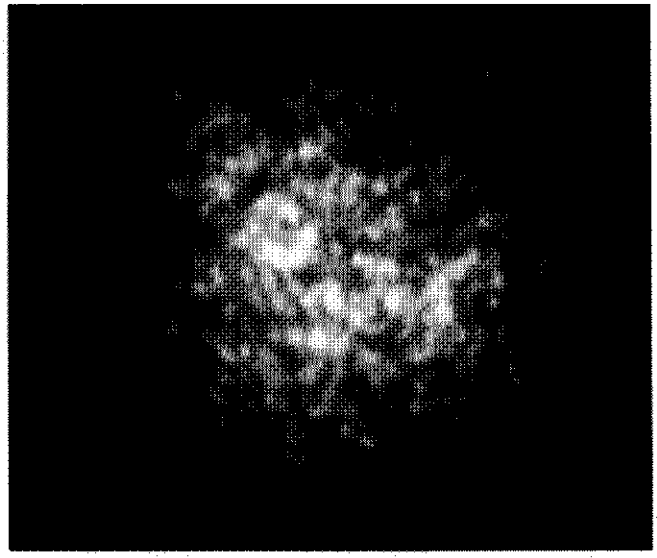

Fig. 8. One of the 100 evaluated speckle interferograms of ω Leonis

Table 1. Mean photometric errors of images reconstructed from computer generated speckle interferograms (n.a. means not available)

data set	recursive	iterative
	100 photoevents/frame	
1	4.9% (±0.8)	4.3% (±1.9)
2	5.3% (±1.3)	1.8% (±0.5)
3	6.8% (±1.0)	4.0% (±1.6)
	50 photoevents/frame	
1	n.a.	10.8% (±2.1)
2	12.1% (±3.3)	6.1% (±1.4)
3	7.8% (±2.4)	4.2% (±1.7)
	25 photoevents/frame	
1	n.a.	11.9% (±3.8)
2	n.a.	13.3% (±3.3)
3	n.a.	14.4% (±5.8)

Figure 8 is one of the 100 evaluated speckle interferograms of ω Leonis. Figure 9 shows two diffraction-limited reconstructions. Figure 9a is the image reconstructed with the building block method and 400 iteration steps, and Fig. 9b is the image obtained from the same object bispectrum by the recursive phase reconstruction method. Fig. 10 shows the decreasing distance function between the measured object bispectrum $O^{(3)}(u, v)$ and the bispectrum $O_k^{(3)}(u, v)$ of the iterated image of step k during the reconstruction of the image shown in Fig. 9a.

5.3. *Building block reconstruction of η Carinae*

Figure 11 shows a diffraction-limited image of η Carinae reconstructed by speckle masking and the building block method. This image was reconstructed from the same 300 speckle inter-

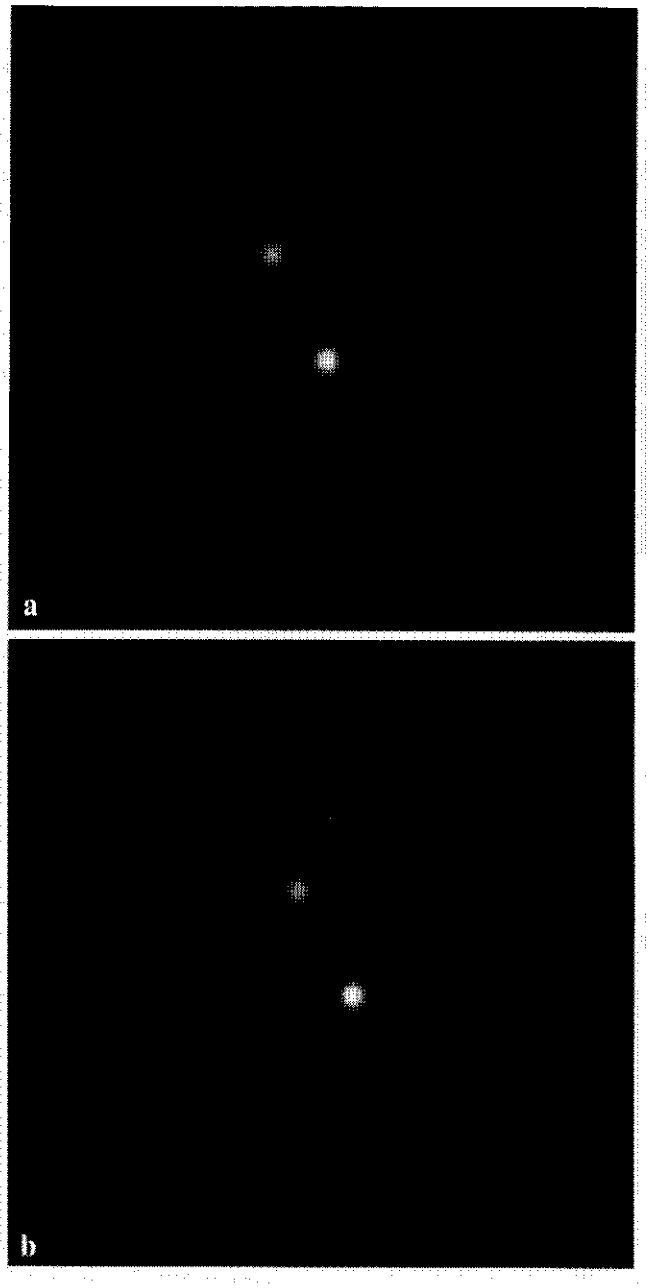

Fig. 9. a and b. Two diffraction-limited images reconstructed from the average bispectrum of 100 speckle interferograms of ω Leonis (see Fig. 8). **a** (top) is the reconstruction obtained with the building block method and 400 iterations. **b** (bottom) shows the image reconstructed from the same bispectrum with the conventional recursive method. The separation of the two stars is 0.″46

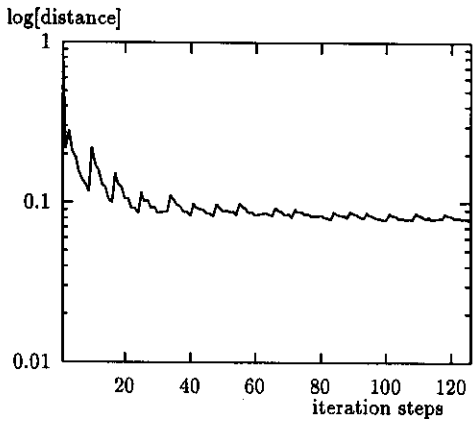

Fig. 10. Convergence curve of the building block reconstruction of ω Leonis shown in Fig. 9a. The measured distance is displayed with a logarithmic scale (arbitrary scaling factor) as a function of the iteration steps

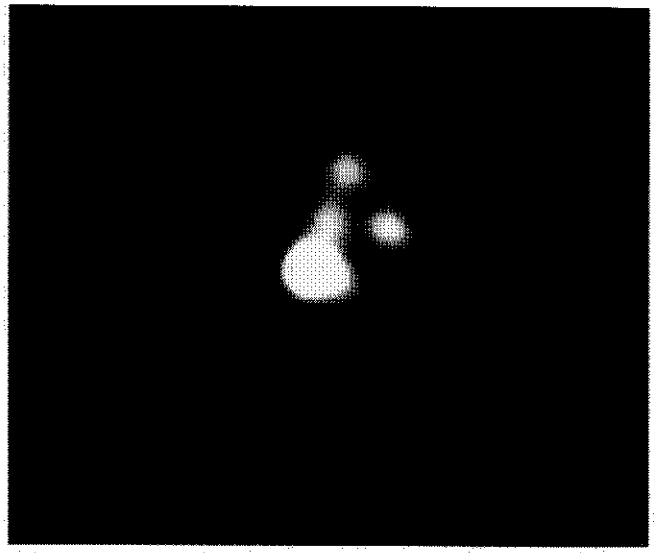

Fig. 11. Diffraction-limited image reconstructed from the average bispectrum of 300 speckle interferograms of *eta* Carinae by the building block method and 2000 iteration steps. The image of η Carinae consists of one dominant star and three objects at separations of 0.″21, 0.″18, and 0.″11; the three faint objects are ~12-times fainter than the dominant star (north is at the top and east to the left)

ferograms as used for the first speckle masking observation of η Carinae (Hofmann & Weigelt 1988). The diffraction-limited images of η Carinae reconstructed from the average bispectrum by (a) the recursive method (Hofmann & Weigelt 1988) and by (b) the building block method (Fig. 11) show one dominant star and three fainter objects at separations 0.″21, 0.″18, and 0.″11. The three faint objects are ~12-times fainter than the dominant star.

The SNR of the bispectrum of η Carinae and ω Leonis is approximately equal to the SNR of the bispectrum in the computer experiment with photon noise corresponding to ~100 photoevents per frame (Sect. 5.1). In this computer simulation the mean photometric error in the reconstruction was about 4%. Therefore, the SNR in the η Carinae and ω Leonis reconstructions is similar, but not identical because of differences in seeing and other differences.

6. Summary

We have investigated an iterative least-squares method for reconstructing diffraction-limited images from the object bispectrum. We have shown theoretically and by image reconstruction experiments that the iteration process converges to the correct image of the object. Furthermore, the experiments performed with computer-generated speckle-interferograms suggest that the presented iterative method yields reconstructions with higher photometric quality than the recursive method (at least in computer simulations). Finally, we have discussed the application of modified methods to speckle interferometry, the Knox-Thompson method, imaging shearing interferometry, deconvolution of aberrated images, the nonredundant mask method, tomography, radio interferometry and optical long-baseline interferometry.

Acknowledgements. We thank W. Barth for helping in the computer experiments, and B. Sherwood, R. Porcas and I. Pauliny-Toth for carefully reading the manuscript.

Appendix A

In this appendix we derive the approximated expression of the distance function $d_{k+1}(x')$ given in Eq. (7). We consider only terms linear in $1/k$, i.e. the approximation of $d_{k+1}(x')$ is based on the fact that the iterated image already consists of a large number k of building blocks. The Fourier transform of the image after iteration step $k+1$ can be described by

$$O'_{k+1}(u) = O'_k(u) + \exp\{-2\pi i u\, x'\}, \tag{A1}$$

where x' is the position of the $(k+1)$th building block $t(x-x') = \delta(x-x')$ (for the sake of simplicity and without sacrifying generality $t(x)$ is replaced by a Dirac Delta function) and where $O'_{k+1}(0) = k+1$ and $O'_k(0) = k$ is valid. The normalized version of $O'_{k+1}(u)$ is called $O_{k+1}(u)$ (with $O_{k+1}(0) = 1$) and is given by

$$O_{k+1}(u) = \frac{1}{k+1}\,[\,O'_k(u) + \exp\{-2\pi i u\, x'\}\,]$$

$$= \frac{k}{k+1}\,[\,O_k(u) + \frac{1}{k}\exp\{-2\pi i u\, x'\}\,], \tag{A2}$$

with $O_k(0) = 1$. For $k \gg 1$, we can use the approximation

$$O_{k+1}(u) \approx O_k(u) + \frac{1}{k}\exp\{-2\pi i u\, x'\}. \tag{A3}$$

Using this equation the bispectrum $O^{(3)}_{k+1}(u,v)$ can be written as

$$\begin{aligned} O^{(3)}_{k+1}(u,v) \approx\ & [\,O_k(u) + \frac{1}{k}\exp\{-2\pi i u\, x'\}\,] \\ & \times [\,O_k(v) + \frac{1}{k}\exp\{-2\pi i v\, x'\}\,] \\ & \times [\,O_k(-u-v) + \frac{1}{k}\exp\{2\pi i (u+v)\, x'\}\,]. \end{aligned} \tag{A4}$$

Since for $k \gg 1$ only the terms linear in $1/k$ are relevant, Eq. (A4) can be rewritten by

$$\begin{aligned} O^{(3)}_{k+1}(u,v) \approx\ & O^{(3)}_k(u,v) \\ & + \frac{1}{k}\,O_k(u)\,O_k(v)\,\exp\{+2\pi i (u+v)\, x'\} \\ & + \frac{1}{k}\,O_k(u)\,O_k(-u-v)\,\exp\{-2\pi i v\, x'\} \\ & + \frac{1}{k}\,O_k(v)\,O_k(-u-v)\,\exp\{-2\pi i u\, x'\}, \end{aligned}$$

and

$$\begin{aligned} O^{(3)}_{k+1}(u,v) \approx\ & O^{(3)}_k(u,v) + \frac{1}{k}\,T(u,v;x') \\ & + \frac{1}{k}\,T(u,-u-v;x') + \frac{1}{k}\,T(v,-u-v;x'), \end{aligned} \tag{A5}$$

where we have used the substitution $T(u,v;x') := O_k(u)\,O_k(v)\,\exp\{+2\pi i (u+v)\, x'\}$. The distance function $d_{k+1}(x')$ is defined by

$$\begin{aligned} d_{k+1}(x') &= \int |O^{(3)}(u,v) - O^{(3)}_{k+1}(u,v)|^2\,\mathrm{d}u\,\mathrm{d}v \\ &= \int |O^{(3)}(u,v)|^2\,\mathrm{d}u\,\mathrm{d}v + \int |O^{(3)}_{k+1}(u,v)|^2\,\mathrm{d}u\,\mathrm{d}v \\ &\quad - \int O^{(3)}(-u,-v)\,O^{(3)}_{k+1}(u,v)\,\mathrm{d}u\,\mathrm{d}v - c.c., \end{aligned} \tag{A6}$$

where $c.c.$ denotes the conjugate complex of the expression before. For $k \gg 1$ the term $|O^{(3)}_{k+1}(u,v)|^2$ can be approximated (using Eq. (A5)) by

$$\begin{aligned} |O^{(3)}_{k+1}(u,v)|^2 \approx\ & |O^{(3)}_k(u,v)|^2 \\ & + O^{(3)}_k(-u,-v) \\ & \times \frac{1}{k}\,[\,T(u,v;x') + T(u,-u-v;x') \\ & + T(v,-u-v;x')\,] + c.c.\,. \end{aligned} \tag{A7}$$

The approximated expression of $O^{(3)}(-u,-v)\,O^{(3)}_{k+1}(u,v)$ for $k \gg 1$ has the form

$$O^{(3)}(-u,-v)\,O^{(3)}_{k+1}(u,v) \approx O^{(3)}(-u,-v)\,O^{(3)}_k(u,v)$$

$$+O^{(3)}(-u,-v)\times\frac{1}{k}\,[\,T(u,v;x')+T(u,-u-v;x')$$

$$+T(v,-u-v;x')\,]. \qquad \text{(A8)}$$

Using Eqs. (A6), (A7) and (A8), $d_{k+1}(x')$ can be expressed by

$$d_{k+1}(x') \approx d_k + \frac{1}{k}\int [\,O_k^{(3)}(-u,-v)-O^{(3)}(-u,-v)\,] \times[\,T(u,v;x')+\ldots\,]\,\mathrm{d}u\,\mathrm{d}v \;+\; c.c., \qquad \text{(A9)}$$

where d_k is the distance between the measured bispectrum $O^{(3)}(u,v)$ and the bispectrum $O_k^{(3)}(u,v)$ of the iterated image $o_k(x)$. The integrand of the integral in Eq. (A9) is a hermitian function. Since the integration is performed within the whole uv-plane the integral has a real value and Eq. (A9) is rewritten by

$$d_{k+1}(x') \approx d_k + \frac{2}{k}\int [\,O_k^{(3)}(-u,-v)-O^{(3)}(-u,-v)\,] \times[\,T(u,v;x')+\ldots\,]\,\mathrm{d}u\,\mathrm{d}v. \qquad \text{(A10)}$$

The bispectrum has the following symmetry relations:

$$\begin{aligned} O^{(3)}(-u,-v) &= O(-u)\,O(-v)\,O(u+v) \\ O^{(3)}(-u,u+v) &= O(-u)\,O(u+v)\,O(-v) = O^{(3)}(-u,-v) \\ O^{(3)}(-v,u+v) &= O(-v)\,O(u+v)\,O(-u) = O^{(3)}(-u,-v) \end{aligned} \qquad \text{(A11)}$$

Using the above symmetry relations, Eq. (A10) can be expressed by

$$\begin{aligned} d_{k+1}(x') \approx\; & d_k \\ & + \frac{2}{k}\int [\,O_k^{(3)}(-u,-v)-O^{(3)}(-u,-v)\,] \times T(u,v,x')\,\mathrm{d}u\,\mathrm{d}v \\ & + \frac{2}{k}\int [\,O_k^{(3)}(-u,u+v)-O^{(3)}(-u,u+v)\,] \times T(u,-u-v,x')\,\mathrm{d}u\,\mathrm{d}v \\ & + \frac{2}{k}\int [\,O_k^{(3)}(-v,u+v)-O^{(3)}(-v,u+v)\,] \times T(v,-u-v,x')\,\mathrm{d}u\,\mathrm{d}v. \end{aligned} \qquad \text{(A12)}$$

The integrands of the three above integrals are identical, only the integration variables are different. Since the integration is performed within the whole uv-plane the three integrals yield the same result and Eq. (A12) can be replaced by

$$d_{k+1}(x') \approx d_k + \frac{6}{k}\int [\,O_k^{(3)}(-u,-v)-O^{(3)}(-u,-v)\,] \times O_k(u)\,O_k(v)\,\exp\{+2\pi i(u+v)\,x'\}\,\mathrm{d}u\,\mathrm{d}v, \qquad \text{(A13)}$$

where we have used the identity
$T(u,v;x') := O_k(u)\,O_k(v)\,\exp\{+2\pi i(u+v)\,x'\}$.

Appendix B

In this appendix we discuss the convergence of the proposed iterative image reconstruction algorithm. For the following calculations we assume a noise-free object bispectrum $O^{(3)}(u,v)$. We also assume that the iterated image of step k already consists of a large number k of building blocks ($k \gg 1$) which allows us to use the approximated expression of the distance function $d_{k+1}(x')$ given in Eqs. (7) and (A13). The algorithm converges to the correct image of the object if the distance $d_{k+1}(x')$ between the measured bispectrum and the bispectrum of the iterated image decreases with the number of iteration steps. A sufficient convergence criterion is

$$d_{k+N}(x_{\min}^{k+N}) < d_k(x_{\min}^k), \qquad \text{(B1)}$$

where $d_{k+N}(x_{\min}^{k+N})$ and $d_k(x_{\min}^k)$ are the distance after iteration step $k+N$ (for $N \gg 1$, not for all N) and k, and where $x_{\min}^{k+N}$ and $x_{\min}^k$ denote the positions of the minima in the corresponding distance functions. The convergence criterion given in Eq. (B1) means: the building block method converges if the distance $d_k(x_{\min}^k)$ decreases only after each Nth (for $N \gg 1$) iteration step, and it is not necessary that the distance decreases from iteration step to iteration step. Because of $k \gg 1$ we can use the approximated expression of $d_{k+1}(x')$ given in Eq. (A13) which can be rewritten as

$$d_{k+1}(x') \approx d_k(x_{\min}^k) + a_k(x',x'). \qquad \text{(B2)}$$

From Eq. (A13) we see that the above function $a_k(x,y)$ has the form

$$\begin{aligned} a_k(x,y) &:= \frac{6}{k}\int [O_k^{(3)}(-u,-v) - O^{(3)}(-u,-v)] \times O_k(u)\,O_k(v)\,\exp\{2\pi i(u\,x+v\,y)\}\,\mathrm{d}u\,\mathrm{d}v \\ &= \frac{6}{k}\,[o_k^{(3)}(-x,-y) - o^{(3)}(-x,-y)] \otimes [o_k(x)\,o_k(y)], \end{aligned}$$

where $\otimes$ denotes the convolution operator. $o_k^{(3)}(x,y)$, $o^{(3)}(x,y)$ and $o_k(x)$ are the Fourier transforms of $O_k^{(3)}(u,v)$, $O^{(3)}(u,v)$ and $O_k(u)$, respectively. $o^{(3)}(x,y)$ denotes the measured object triple correlation and $o_k^{(3)}(x,y)$ the triple correlation of the iterated image $o_k(x)$. The functions mentioned are normalized with $\int o_k^{(3)}(x,y)\,\mathrm{d}x\mathrm{d}y = \int o^{(3)}(x,y)\,\mathrm{d}x\mathrm{d}y = \int o_k(x)\,\mathrm{d}x = 1$. Using Eq. (B2) the distance $d_{k+N}(x_{\min}^{k+N})$ at iteration step $k+N$ can be expressed by

$$d_{k+N}(x_{\min}^{k+N}) \approx d_k(x_{\min}^k) + \sum_{i=1}^{N} a_{k+i-1}(x_{\min}^{k+i}, x_{\min}^{k+i}), \qquad \text{(B3)}$$

where $x_{\min}^{k+i}$ denotes the minimum positions of the functions $a_{k+i-1}(x',x')$ for $i = 1\ldots N$. Using Eq. (B3) the convergence criterion given in Eq. (B1) can also be described by

$$\sum_{i=1}^{N} a_{k+i-1}(x_{\min}^{k+i}, x_{\min}^{k+i}) < 0. \qquad \text{(B4)}$$

In other words, the building block method converges, if the sum over the minima of the functions $a_{k+i-1}(x', x')$ for $i = 1...N$ is negative for all iteration steps k.

$a_k(x, y)$ is the convolution of the triple correlation difference $b_k(x, y) := o_k^{(3)}(-x, -y) - o^{(3)}(-x, -y)$ with the positive function $f_k(x, y) := o_k(x)\, o_k(y)$. The non-zero values of $f_k(x, y)$ are distributed within a square of size D (D=extension of $o_k(x)$). $f_k(x, y)$ is centered at $(x = x_0, y = x_0)$, where x_0 denotes the centre of $o_k(x)$. If, for example, $o_k(x) = \delta(x - x_0)$ then $f_k(x, y) = \delta(x - x_0)\,\delta(y - x_0)$. Because of the convolution with $f_k(x, y)$, $a_k(x, y)$ is a smoothed version of $b_k(x, y)$. Since $f_k(x, y)$ is a spatially restricted (extension$\leq$D) positive function centered on the diagonal line $y = x$ at $(x = x_0, y = x_0)$, $a_k(x, x)$ mainly consists of the diagonal elements of $b_k(x, y)$, i.e. $b_k(x, x)$. Using the definition of the triple correlation (Lohmann et al. 1983), $b_k(x, x)$ reads as

$$\begin{aligned} b_k(x, x) &= \int [o_k(x')o_k(x' + x)o_k(x' + x) \\ &\qquad - o(x')o(x' + x)o(x' + x)]\, \mathrm{d}x' \\ &= o_k(x) * |o_k(x)|^2 - o(x) * |o(x)|^2, \end{aligned} \tag{B5}$$

where the asterix $*$ denotes the cross correlation operator. Since in nearly all cases $o_k(x) \neq o(x)$, with $\int o_k(x)\, \mathrm{d}x = \int o(x)\, \mathrm{d}x$, is valid, it is evident that the difference function $b_k(x, x)$ (Eq. (B5)) very often consists of negative values. The same is also true for $a_k(x, x)$ since it is a smoothed version of $b_k(x, x)$ (smoothed by the spatially restricted positive function $f_k(x, y)$). Therefore, it is evident that the sum over the minima of the functions $a_{k+i+1}(x', x')$ for $i = 1...N$ is negative for iteration step k and a large enough N. This means that the convergence criterion given in Eq. (B4) is fullfilled and it is shown that the building block method converges to the correct image of the object.

References

Baier G., Weigelt G. 1983, A&A 121, 137

Baldwin J.E., Haniff C.A., Mackay C.D., Warner P.J. 1986, Nature 320, 595

Cornwell T.J., Wilkinson P.N., 1981, MNRAS 196, 1067

Cornwell T.J. 1987, A&A 180, 269

Cornwell T.J. 1989, Science 245, 263

Dainty J.C. 1984, Stellar Speckle Interferometry, in: Laser Speckle and Related Phenomena, Topics in Applied Physics, Vol.9, ed. J.C. Dainty (Springer, Berlin) ch.7

Freeman J.D., Christou J.C., Roddier F., Mc.Carthy D.W., Cobb M.L. 1988, J. Opt. Soc. Am. A 5, 406

Freeman J.D. et al. 1992, Applications of robust techniques to model fitting of IR speckle results of binary and extended sources, in: *High Resolution Imaging by Interferometry II*, 14-18 Oct. 1991, Beckers J.M. & Merkle F. (eds.), European Southern Observatory, Garching, Germany, (in press)

Glindemann A., Lane R.G., Dainty J.C. 1992, J. Opt. Soc. Am. A 9, 543

Gorham P.W., Ghez A.M., Kulkarni S.R., Nakajima T., Neugebauer G., Oke J.B., Prince T.A. 1989, AJ 98, 1783

Haniff C.A. 1990, J. Opt. Soc. Am. A 8, 134

Hofmann K.-H., Weigelt G. 1986, A&A 167, L15

Hofmann K.-H., Weigelt G. 1986, Appl. Opt. 25, 4280

Hofmann K.-H., Weigelt G. 1990, *Digital Image Synthesis and Inverse Optics*, Gmitro A.F., Idell P.S., LaHaie I.J. (eds.), Proc. SPIE 1351 pp. 522

Hofmann K.-H., Weigelt G. 1990, *Optics in Complex Systems*, Lanzl F., Preuss H.-J., Weigelt G. (eds.), Proc. SPIE 1319, pp. 444

Hofmann K.-H. 1990, *Optics in Complex Systems*, Lanzl F., Preuss H.-J., Weigelt G. (eds.), Proc. SPIE 1319, pp. 457

Hofmann K.-H. 1993, J. Opt. Soc. Am. A 10, 329

Hofmann K.-H., Weigelt G. 1992, Building block method: image reconstruction from the bispectrum using an iterative algorithm, in: *High Resolution Imaging by Interferometry II*, 14-18 Oct. 1991, Beckers J.M. & Merkle F. (eds.), European Southern Observatory, Garching, Germany, pp. 193

Knox K.T., Thompson B.J. 1974, ApJ 193, L45

Labeyrie A. 1970, A&A 6, 85

Lannes A. 1988, in: Proc. of the NOAO/ESO Workshop on *High-Resolution Imaging by Interferometry*, Garching, Germany, 15-18 March 1988, Merkle F. (ed.), ESO Garching, Germany, pp.169

Lannes A. 1990, J. Opt. Soc. Am. A 7, 500

Lohmann A.W., Weigelt G., Wirnitzer B. 1983, Appl. Opt. 22, 4028

Marron J.C., Sanchez P.P., Sullivan R.C. 1990, J. Opt. Soc. Am. A 7, 14

Meng J., Aitken G.J.M., Hege E.K., Morgan J.S. 1990, J. Opt. Soc. Am. A 7, 1243

Morita K.-I. 1991, *Radio Interferometry: Theory, Techniques and Applications*, IAU Coll. 131, ASP Conference Series, Cornwell T.J. and Perley R.A. (eds.), Vol. 19, pp. 197

Nakajima T., Kulkarni S.R., Gorham P.W., Ghez A.M., Neugebauer G., Oke J.B., Prince T.A., Readhead A.C.S. 1989, AJ 97, 1510

Pauliny-Toth I.I.K., Preuss E., Witzel A., Kellermann K.I., Shaffer D.B., Purcell G.H., Grove G.W., Jones D.L., Cohen M.H., Moffet A.T., Romney J., Schilizzi R.T., Rinehart R. 1976, Nature 259, 17

Pearson T.J., Readhead A.C.S. 1984, ARA&A 22, 97

Pehlemann E., Hofmann K.-H., Weigelt G. 1992, A&A 256, 701

Pratt W.K. 1978, *Digital Image Processing*, Wiley, New York

Readhead A.C.S., Wilkinson P.N., 1978, ApJ 223, 25

Readhead A.C.S., Nakajima T., Pearson T.J., Neugebauer G., Oke J.B., Sargent W.L.W. 1988, AJ 95, 1278

Reinheimer T., Hofmann K.-H., Weigelt G. 1992, Computer simulations of interferometric imaging with the VLT interferometer, in: *High Resolution Imaging by Interferometry II*, 14-18 Oct. 1991, Beckers J.M. & Merkle F. (eds.), European Southern Observatory, Garching, Germany, pp. 827

Reinheimer T., Hofmann K.-H., Weigelt G. 1993, Interferometric imaging with arrays of large optical telescopes in the multi-speckle mode, A&A (submitted)

Ribak E. 1987, Appl. Opt. 26, 197

Roddier F. 1981, Progress in Optics, Wolf E. (ed.) 19, 281

Roddier F., Roddier C. 1986, Opt. Commun. 66, 350

Schwab F., 1980, Proc. SPIE 231, 18

Takajo H., Takahashi T. 1991, J. Opt. Soc. Am. A 8, 1038

Weigelt G. 1977, Opt. Commun. 21, 55

Weigelt G., Wirnitzer B. 1983, Opt. Lett. 8, 389

Weigelt G. 1991, Progress in Optics, Wolf E. (ed.) 29, 295

Wirnitzer B. 1985, J. Opt. Soc. Am. A 2, 14

This article was processed by the author using Springer-Verlag LaTeX A&A style file version 3.